IOP Publishing Nanotechnology
Nanotechnology 27 (2016) 224002 (7pp) doi:10.1088/0957-4484/27/22/224002

Integrated plasmonic metasurfaces for spectropolarimetry

Wei Ting Chen[1], Peter Török[2], Matthew R Foreman[3], Chun Yen Liao[1], Wei-Yi Tsai[1], Pei Ru Wu[1] and Din Ping Tsai[1,4]

[1] Department of Physics, National Taiwan University, Taipei 10617, Taiwan
[2] Blackett Laboratory, Department of Physics, Imperial College London, London, SW7 2BW, UK
[3] Max Planck Institute for the Science of Light, Günther-Scharowsky-Straße 1, D-91058 Erlangen, Germany
[4] Research Center for Applied Sciences, Academia Sinica, Taipei 11529, Taiwan

E-mail: peter.torok@imperial.ac.uk and dptsai@sinica.edu.tw

Received 7 December 2015
Accepted for publication 5 April 2016
Published 26 April 2016

Abstract

Plasmonic metasurfaces enable simultaneous control of the phase, momentum, amplitude and polarization of light and hence promise great utility in realization of compact photonic devices. In this paper, we demonstrate a novel chip-scale device suitable for simultaneous polarization and spectral measurements through use of six integrated plasmonic metasurfaces (IPMs), which diffract light with a given polarization state and spectral component into well-defined spatial domains. Full calibration and characterization of our device is presented, whereby good spectral resolution and polarization accuracy over a wavelength range of 500–700 nm is shown. Functionality of our device in a Müller matrix modality is demonstrated through determination of the polarization properties of a commercially available variable waveplate. Our proposed IPM is robust, compact and can be fabricated with a single photolithography step, promising many applications in polarization imaging, quantum communication and quantitative sensing.

S Online supplementary data available from stacks.iop.org/nano/27/224002/mmedia

Keywords: surface plasmon, metasurfaces, metamaterials, spectropolarimetry

(Some figures may appear in colour only in the online journal)

1. Introduction

Optics is an important tool to quantitatively interrogate a broad variety of physical systems and processes, information of which can be extracted through analysis of the optical intensity, polarization and wavelength of light. Analysis of the polarization of light can, for example, furnish details regarding sample structure [1] and material properties [2], whereas spectroscopic measurements carry information regarding chemical composition [3], particle velocity [4], local magnetic and electric fields [5, 6] and more [7]. Simultaneous polarization and spectral measurements, i.e. spectropolarimetry, combines the power of both techniques and constitutes a more exhaustive analytic tool since the information carried by these channels are typically uncorrelated. Accordingly such measurements have seen employ in many branches of science including for example astrophysics [8, 9], cosmology [10], remote sensing [11], biophysics [12] and data storage [13].

Spectropolarimetry can be practically realized using a number of experimental architectures, which differ through the means of spectral and polarization discrimination. Seperation of individual spectral components is typically achieved by means of either a tunable optical filter [14] or a dispersive element, such as a prism or grating structure [15]. Differing polarization components, on the other hand, can be found using sequential measurements with variable waveplates and analyzers [16] or simultaneously by means of division of amplitude polarimeters [17] or polarization gratings [18, 19]. So-called channeled spectropolarimeters represent a further option in which interferometrically generated carrier frequencies are amplitude modulated according

to the state of polarization [20], thereby allowing both spectral and polarization information to be obtained in a single snapshot [21].

Each spectropolarimeteric architecture brings its own set of advantages and disadvantages according to the specific application at hand (see e.g. [11] for a fuller discussion). For example, sequential measurements using variable elements (e.g. filters or polarization analyzers) are unsuitable for scenarios in which the spectral or polarization content can vary over the course of a measurement. Commonly, such elements are solid-state or liquid crystal based which can be both costly and bulky. Additionally, use of rotating or variable elements can introduce mechanical vibrations, wear and a potentially undesirable energy overhead. The working regime of liquid crystal based elements is also generally limited to the visible or near-infrared [19, 22] and thus can not be employed in the infra-red or terahertz regime. Channeled spectropolarimeters avoid the need for sequential measurements however require more involved data analysis and hence computational resources, and moreover, suffer from a loss of spectral resolution due to use of multiple spectral bands to derive the complete polarization state [20]. Grating based systems, similarly, allow simultaneous measurements but can suffer from lower signal levels and can involve complicated fabrication processes making them less suitable for device integration.

Plasmonic metasurfaces, i.e. nano-structured thin metallic films, are promising candidates for development of compact photonic devices for spectropolarimetry, since they afford simultaneous control over the phase, momentum, amplitude and polarization of light [23–25]. These attributes have accordingly attracted much interest with subsequent realization of many metasurface-based optical elements, such as beam steerers, polarizers, waveplates, modulators, holograms and others [26–35]. Polarization selective plasmonic metasurfaces have also been reported [36–39], with one shot polarization measurements using three interweaved plasmonic metasurfaces reported [40] during the preparation of this article. In this work, we propose and demonstrate the use of six integrated plasmonic metasurfaces (IPMs) for spectropolarimetry hence extending the functionality of earlier designs. Our IPM design, which is detailed in section 2, allows many of the limitations of conventional spectropolarimetry methods to be overcome. Moreover, due to its compact size our IPM device allows for direct on-camera integration [37, 38, 41, 42]. In section 3 we describe the fabrication process of our IPM device which is fully compatible with today's industry manufacturing technologies, before detailing its characterization over the wavelength range of 500–700 nm in section 4. Finally, we experimentally demonstrate the functionality of the IPM device through determination of the polarization properties of a commercially available waveplate, before concluding in section 5.

2. Principle and design

Complete characterization of (possibly partially) transversally homogeneously polarized light of a given wavelength can only be achieved via analysis of the relative intensity of multiple distinct polarization components. Practical realization of a spectropolarimetric metadevice therefore requires steering of different input polarization and spectral components into distinct directions as depicted schematically in figure 1(a). Polarization selective diffractive steering can be achieved using plasmonic metasurfaces consisting of suitably designed nanorod arrays (see figures 1(b) and 2) as detailed below, while the intrinsic dispersive behavior automatically affords angular multiplexing of different spectral components. Upon collection of the light diffracted from the IPM, e.g. using a camera or multiple photodiodes, the polarization state, parameterized by a Stokes vector $\vec{S} = (S_0, S_1, S_2, S_3)$ can be determined as a function of wavelength [43] (see figure 1(c)). A minimum of four measurements are required to ensure that the retrieval of the polarization information is not underdetermined, therefore requiring at least four metasurfaces. Device performance, however, scales with the number of metasurfaces [44, 45] due to increased redundancy in the measurements, such that we elect to use an optimal design consisting of six metasurfaces arranged in a 2×3 array corresponding to horizontal (0°), vertical (90°), ±45°, right (RCP) and left circular polarization (LCP) analyzers (see figures 1 and 2).

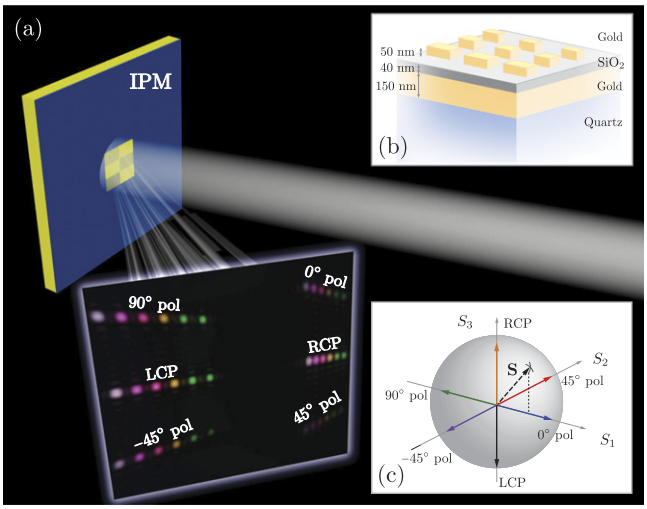

Figure 1. Illustration of our IPM device. A 2×3 array of metasurfaces acting as differing polarization state analyzers separates input light into its constituent polarization and spectral components. Experimental image shown was obtained for input $-45°$ linearly polarized light with six spectral components. (b) Quasi-planar structure of each metasurface. (c) Schematic of polarimetric 'triangulation' in polarization space, whereby a given polarization state (dashed arrow) is projected onto a basis of six measurement states (solid colored arrows). Note that $S_1^2 + S_2^2 + S_3^2 \leqslant S_0^2$ such that Stokes vectors must lie within the so-called Poincaré sphere.

Each metasurface consists of rows of gold nanorods arranged periodically in the horizontal (x) direction (with period Λ) as shown in figure 2 and patterned on a 40 nm thick SiO_2 layer on a gold mirror, yielding a total thickness of 260 nm excluding substrate (see figure 1(b)). A reflection modality was adopted due to the greater optical efficiency it confers and the thickness of the SiO_2 chosen so as to

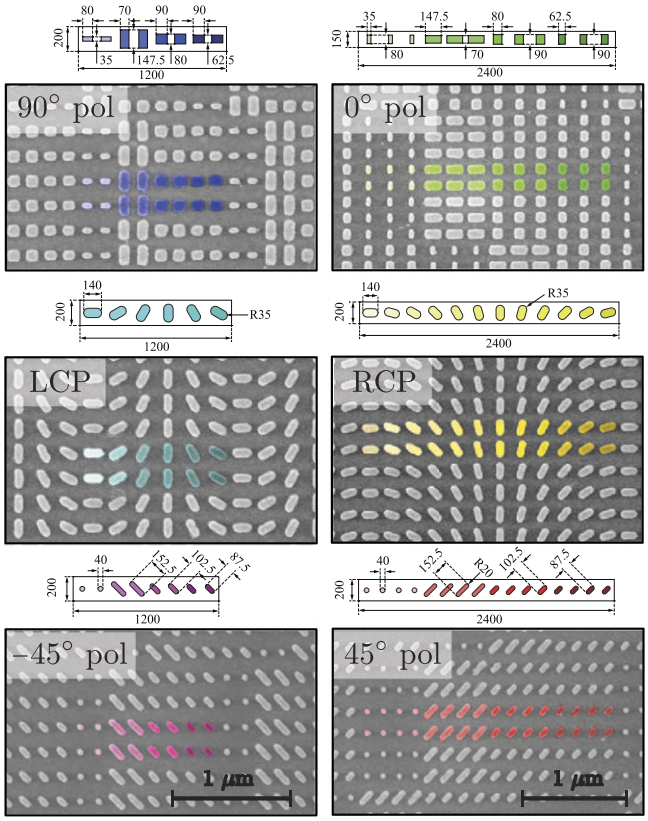

Figure 2. Main panels show scanning electron microscope images of regions of the fabricated plasmonic metasurfaces and are labeled with the corresponding polarization state analyzed by each. Schematics of the nominal designs of a single unit cell are also shown. A pseudo-color gradient has been superimposed to depict the linear phase gradient across the unit cell at $\lambda = 700$ nm.

maximize the reflectance of the linear polarization channels, which is lower than in the circular channels [27, 46–48]. We note that although metasurfaces approximately 72 μm × 48 μm in size were used, the dimensions are scalable to 2.4 μm × 2.4 μm by reduction of the number of constituent unit cells to help avoid potential spatial coherence related issues.

Interaction of an incident electromagnetic wave with each metasurface can be modeled using the generalized Snell's law [25], whereby, $kn_i(\sin\theta_r - \sin\theta_i) = \mathrm{d}\Phi/\mathrm{d}x$ where $k = 2\pi/\lambda$ is the vacuum wavenumber, λ is the wavelength, n_i is the refractive index of the surrounding medium, $\theta_{i,r}$ are the angles of incidence and reflection respectively and Φ is the interfacial phase discontinuity imposed by the metasurface upon reflection. Continuous tuning of the phase discontinuity can be achieved across each unit cell by variation of the length, width or orientation of each constituent nanorod, which in turn controls the spectral position and excitation strength of the plasmonic eigenmodes (see supporting information 1). To steer the incident light into a well-defined direction, we therefore engineer the phase anisotropy so that a specific incident polarization sees a constant gradient $\mathrm{d}\Phi/\mathrm{d}x = 2\pi/\Lambda$. Full three-dimensional finite element simulations were used to identify suitable structural parameters for each nanorod (see supporting information 1 and 2). The final designs are shown in figure 2. For metasurfaces acting as linear analyzers, only the length and width of each nanorod was varied (four distinct geometries were used in each unit cell), while for the LCP and RCP channels Φ was controlled through variation of the nanorod orientation (6 and 12 different orientations uniformly distributed over 180° were used respectively). Although the linear phase gradient was designed for a nominal wavelength, it exhibits only a weak wavelength dependence, allowing broadband operation as has been previously demonstrated [26, 31, 40]. As a consequence of the linear phase gradient, normally incident light of the desired polarization is diffracted at an angle $\theta_r = \sin^{-1}(\lambda/\Lambda)$, where we have assumed $n_i = 1$ to match our experimental conditions. Calculations of the associated extinction ratios can be found in supporting information 3. Importantly, a dispersive behavior is exhibited such that angular multiplexing of different spectral components is automatically achieved. Angular discrimination of the different polarization components originating from each metasurface was achieved by choosing differing periods of $\Lambda = 1.2$ and 2.4 μm for metasurfaces on the left and right side of the metasurface array. Similarly, a vertical periodicity of 4.8 μm was imposed for the top and bottoms rows to achieve a vertical displacement in the output beams.

3. Fabrication and characterization

Fabrication of our IPM metadevice was performed using a standard e-beam lithography and lift-off process. Specifically a 3 nm thick gold (Au) film was first sputtered onto a quartz wafer. This was followed by thermal evaporation of another 147 nm Au layer to bring the total thickness of the gold layer to 150 nm. The sample was subsequently spin coated with a 260 nm thick SiO_2 (IC1-200, from Futurrex, Inc) layer and baked for 3 min on a 200 °C hotplate. Subsequently, we used reactive ion etching with tetrafluoromethane (CF_4) to reduce the thickness to 40 nm. The sample was then further coated with an e-beam resist (ZEP 520A from ZEON Corporation) of 180 nm thickness, and baked for 3 min on a hotplate at 180 °C. Thereafter the individual plasmonic metasurfaces were defined using an e-beam lithography system (Elionix ELS-7000) using an acceleration voltage of 100 keV and current of 30 pA. After exposure, the sample was developed in a solution of ZED N50 (ZEON Corporation) for 180 s. Once the development of the resist was complete, a 50 nm thick Au film was deposited by electron-beam evaporation. The sample was then soaked in ZEMAC (ZEON Corporation) for over 12 h, before the unpatterned regions were finally removed in an ultrasonic cleaner.

Following fabrication we characterized the metadevice using the experimental setup shown in figure 3(a). Specifically, we used a supercontinuum laser combined with an acousto-optic filter, which outputs a series of discrete, equally spaced laser peaks, i.e. a frequency comb. The desired polarization state was generated by introduction of several polarizers and phase retarders. A thin, uncoated glass plate was also inserted into the collimated light path at near normal

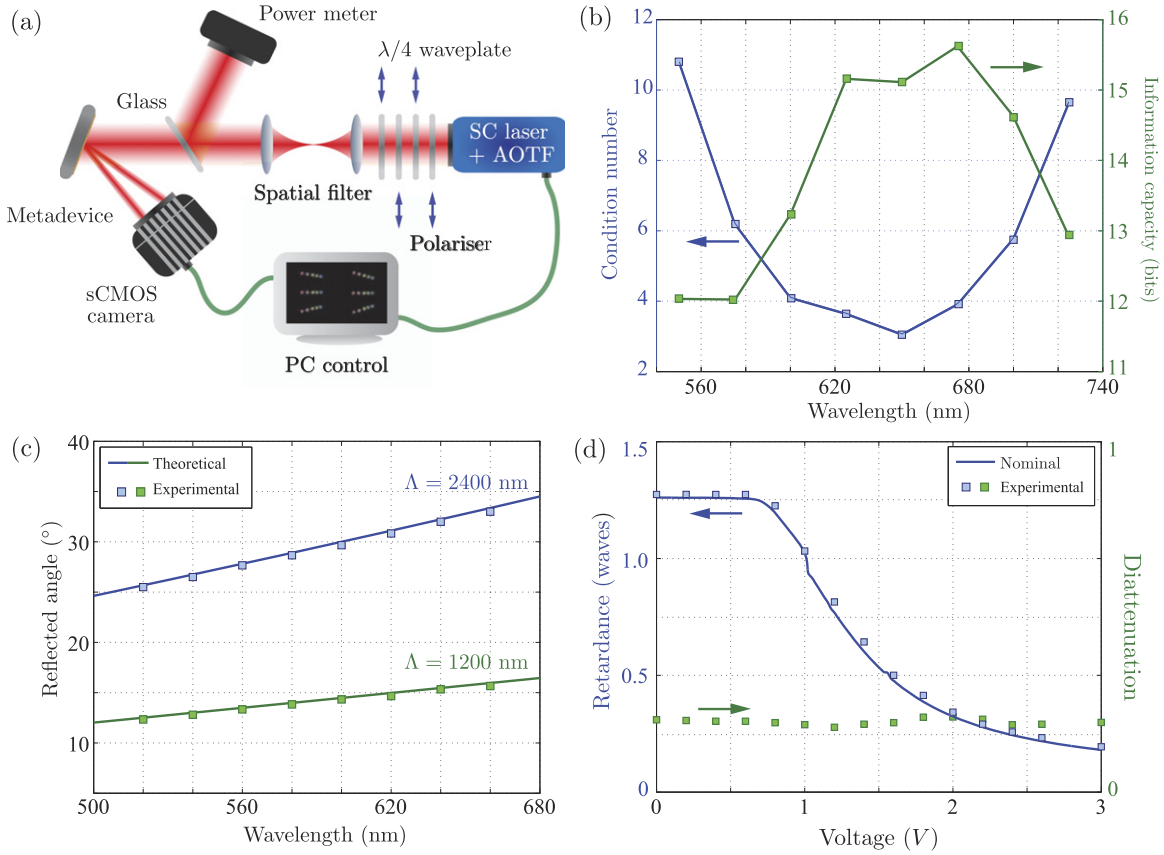

Figure 3. (a) Experimental setup used for characterization of our IPM device. SC: supercontinuum laser. AOTF: acousto-optic filter. (b) Variation of condition number and information capacity as quantified by the logarithm of the number of distinguishable polarization states. (c) Theoretical predictions and experimentally observed spectral dispersion for circular detection channels. (d) Retardance and diattenuation values extracted from measured Mller matrices of a known variable waveplate.

incidence to provide reference intensity measurements for device calibration. Light diffracted by the IPM was directly collected by a sCMOS camera. Figure 1 shows a typical experimental image when the IPM device is illuminated with $-45°$ polarized light. As the incident polarization is varied, so the relative intensity of each intensity peak changes, as can be seen in the Supplementary Movie. To study the polarization response of our metadevice for a given wavelength, we must determine the relationship between the intensity of individual peaks arising from diffraction from each metasurface (which we collect into a vector of intensities $\vec{I}$) and the incident state of polarization $\vec{S}$, which can be written in the form $\vec{I} = \mathbf{A}\vec{S}$ where $\mathbf{A}$ is a 6×4 instrument matrix. To determine $\mathbf{A}$ we followed the procedure detailed in [49] and supporting information 4. This procedure also acts as a calibration for subsequent spectropolarimetric measurements and must be performed for all wavelengths. As an example the experimental instrument matrix found at $\lambda = 650$ nm is

$$\mathbf{A} = \begin{pmatrix} 0.2754 & 0.2287 & 0.0069 & -0.0078 \\ 0.2447 & -0.2033 & 0.0001 & -0.0063 \\ 0.4750 & 0.0037 & 0.0582 & -0.4584 \\ 0.4484 & 0.0183 & -0.0416 & 0.3928 \\ 0.2210 & -0.0005 & 0.1709 & 0.0059 \\ 0.2747 & 0.0110 & -0.2224 & 0.0245 \end{pmatrix}$$

from which it is apparent that the first two rows correspond to a 0° and 90° linear analyzer respectively, the third and fourth to LCP and RCP analyzers and finally the fifth and sixth row to $+45°$ and $-45°$ analyzers, therefore matching the nominal IPM design. Approximately double the power is found in the RCP and LCP channels as compared to the linear channels. This is predicted from numerical calculations of the diffraction efficiencies which are ~36% and 55% for the linear and circular channels respectively. Experimental instrument matrices for alternative wavelengths are given in supporting information 5.

4. Results and discussion

Critically, the instrument matrix affects a number of key performance metrics for the IPM device. Specifically, the condition number of the instrument matrix, $\kappa = \|\mathbf{A}\|\|\mathbf{A}^{-1}\|$ where $\|\cdot\|$ denotes the $p = 2$ matrix norm, quantifies the maximum extent to which noise is amplified during the polarization reconstruction process. Smaller condition numbers are preferable, with our metadevice exhibiting a minimum of 3.028 at $\lambda = 650$ nm (figure 3(b)). Theoretically the minimum achievable condition number is $\kappa = \sqrt{3} \approx 1.732$, corresponding to the nominal design of our metadevice, albeit

with balanced detectors [45]. When the imbalance arising from differing diffraction efficiencies is considered the theoretical condition number of our IPM is ≈ 2.082.

The instrument matrix, in concert with experimental (noisy) intensity data, can also be used to quantify the polarization resolution and hence information capacity of our metadevice. The former describes the precision to which a polarization state can be determined, while the latter dictates the average information gain per measurement (for each wavelength channel and a given data acquisition rate). Calculation of the polarization resolution followed an information theoretic approach based on the Cramer–Rao lower bound [43]. Using this method the volume of uncertainty in polarization space was first calculated from the associated Fisher information matrix, from which the total number of distinguishable polarization states was derived. A Shannon information capacity then follows (see supporting information 6 for further details) and is shown in figure 3(b). At wavelength ~650 nm, the information per measurement of ~15 bits is largest, however drops to ~12 bits per measurement away from this optimal wavelength.

Of further importance for all spectroscopic measurements is the spectral resolution. For our device this is closely related to the angular dispersion, α, and hence period, Λ, of each metasurface. Figure 3(c) compares the theoretical and experimentally measured angular dispersions for the LCP and RCP channels ($\Lambda = 1200$ and 2400 nm respectively). Excellent agreement is evident in both cases with $\alpha \approx 0.053$ and $0.024°/\text{nm}$. Assuming we use our device as the dispersive element in a spectrometer with a focal length of 25 cm focal length and use a CCD detector with $N = 2048$ pixels (pixel width $W_\text{p} = 14\ \mu$m and total width of 28.67 mm), the wavelength spans, $\Delta\lambda$, on the CCD are 123.85 and 273.8 nm respectively. Finally, the spectral resolution follows as $\delta\lambda = (\text{RF} \cdot \Delta\lambda \cdot W_\text{s})/(N \cdot W_\text{p})$, where W_s is the entrance slit width and the resolution factor RF is determined by the relationship between slit width and the pixel width [50]. Assuming typical values of $W_\text{s} \approx 2W_\text{p}$ and RF ≈ 2.5 we find spectral resolutions of 0.3 and 0.67 nm for the LCP and RCP channels. Similar spectral resolutions for the (90°, −45°) and (0°+45°) channels are also found.

Once the system is characterized, spectropolarimetric measurements can readily be performed. The IPM can either be used in the calibration setup or built into a new instrument, such as an ellipsometer or a polarized light microscope. Introduction of a sample before the IPM, however, can modify the incident polarization state as described by the Müller matrix, $\mathbf{M}(\lambda)$, of the sample. With knowledge of the incident polarization the change of polarization can be inferred since the measured intensities are given by $\vec{I}(\lambda) = \mathbf{A}(\lambda)\mathbf{M}(\lambda)\vec{S}$. Moreover, by illuminating the sample-IPM combination with four (or more) differently polarized beams (parameterized by the Stokes vectors $\vec{S}_j$, $j = 1,\ldots,4$, which we combine into a matrix $\mathbf{S} = [\vec{S}_1, \vec{S}_2, \vec{S}_3, \vec{S}_4]$), multiple output intensity vectors $\vec{I}_j(\lambda)$ (which we also combine into a matrix $\mathbf{I}(\lambda)$) result. The resulting matrix equation

$$\mathbf{I}(\lambda) = \mathbf{A}(\lambda)\mathbf{M}(\lambda)\mathbf{S} \tag{1}$$

can be simply inverted, therefore allowing determination of the complete polarization properties of a sample, as contained in the Müller matrix. A well-conditioned instrument matrix is essential for the stability of the inversion. Despite the good conditioning of our IPM device, inaccuracies can arise e.g. from errors in incident polarization states, which in turn give rise to non-physical Müller matrices. Physically admissible Müller matrices were ensured in our work, however, by adopting a constrained maximum-likelihood estimator [51] seeded with a least norm solution of equation (1).

To demonstrate the capabilities of our metadevice we have obtained the Müller matrix of a liquid crystal tunable full waveplate (Thorlabs LCC1223-A) (see supporting information 7). Nominal retardance values at $\lambda = 635$ nm as provided by Thorlabs Inc. are shown in figure 3(d) as a function of applied voltage. Extraction of the retardance of the waveplate from experimental Müller matrices (acquired at $\lambda = 650$ nm) was achieved through a polar decomposition of the associated Müller matrix [52], which represents an arbitrary element as a series of a pure diattenuator, retarder and depolarizer. Experimentally determined retardance values are also shown in figure 3(d) from which good agreement is seen albeit for a small systematic offset attributable to wavelength dependent retardance of the waveplate. A slight parasitic diattenuation is also seen which we believe arises from the liquid crystal nature of the waveplate.

5. Conclusions

In conclusion, by integration of six plasmonic metasurfaces, each engineered to respond differently to specific incident polarization states, we have realized a compact spectropolarimetric device. Dispersive properties of our metadevice allowed simultaneous spectral measurements of incident light to be made, with spectral resolutions of ~0.3 nm easily achievable upon insertion of our IPM device into typical spectrometer setups. Device functionality over a large bandwidth was verified through experimental characterization in terms of the condition number of the associated instrument matrix and the information capacity. Finally, when used in a Müller matrix polarimetric modality, our IPM device accurately reproduced the known polarization properties of a variable waveplate inserted before the IPM. Due to the integrability, compact size, low energy overhead and compatibility with current manufacturing techniques, we envisage that the proposed IPM device can find successful applications in any field employing the polarization of light such as quantitative bioscience, remote sensing, quantum communication and polarization imaging.

Acknowledgments

DPT acknowledges support from the Ministry of Science and Technology, Taiwan (Grants 103-2745-M-002-004-ASP and 103-2911-I-002-594) and Academia Sinica (Grant AS-103-TP-A06). PT was funded via an Academia Sinica Professorial Scholarship. MRF acknowledges support from an Alexander von Humboldt Fellowship and the Max Planck Society. The authors also thank Dr C Macias-Romero (École Polytechnique Fédérale de Lausanne, Switzerland) for discussions.

References

[1] Camacho R, Tubasum S, Southall J, Cogdell R J, Sforazzini G, Anderson H L, Pullerits T and Scheblykin I G 2015 Fluorescence polarization measures energy funneling in single light-harvesting antennas-LH2 vs conjugated polymers *Sci. Rep.* **5** 15080

[2] Hall S A, Hoyle M-A, Post J S and Hore D K 2013 Combined Stokes vector and Mueller matrix polarimetry for materials characterization *Anal. Chem.* **85** 7613–9

[3] Colthup N 2012 *Introduction to Infrared and Raman Spectroscopy* (Amsterdam: Elsevier)

[4] Leutenegger M, Martin-Williams E, Harbi P, Thacher T, Raffoul W, André M, Lopez A, Lasser P and Lasser T 2011 Real-time full field laser doppler imaging *Biomed. Opt. Express* **2** 1470–7

[5] Donati J-F and Landstreet J D 2009 Magnetic fields of nondegenerate stars *Ann. Rev. Astron. Astro.* **47** 333–70

[6] Bublitz G U and Boxer S G 1997 Stark spectroscopy: applications in chemistry, biology, and materials science *Annu. Rev. Phys. Chem.* **48** 213–42

[7] Demtröder W 2013 *Laser Spectroscopy: Basic Concepts and Instrumentation* (Berlin: Springer)

[8] del Toro Iniesta J C 2003 *Introduction to Spectropolarimetry* (Cambridge: Cambridge University Press)

[9] Sterzik M F, Bagnulo S and Palle E 2012 Biosignatures as revealed by spectropolarimetry of earthshine *Nature* **483** 64–6

[10] Giovannini M 2010 Circular dichroism, magnetic knots, and the spectropolarimetry of the cosmic microwave background *Phys. Rev.* D **81** 023003

[11] Tyo J S, Goldstein D L, Chenault D B and Shaw J A 2006 Review of passive imaging polarimetry for remote sensing applications *Appl. Opt.* **45** 5453–69

[12] Volkenstein M V 1977 *Molecular Biophysics* (New York: Academic)

[13] Chon J, Zijlstra P and Gu M 2009 Five-dimensional optical recording mediated by surface plasmons in gold nanorods *Nature* **459** 410–3

[14] Gupta N, Dahmani R and Choy S 2002 Acousto-optic tunable filter based visible- to near-infrared spectropolarimetric imager *Opt. Eng.* **41** 1033–8

[15] Gorodetski Y, Biener G, Niv A, Kleiner V and Hasman E 2005 Space-variant polarization manipulation for far-field polarimetry by use of subwavelength dielectric gratings *Opt. Lett.* **30** 2245–7

[16] Pust N J and Shaw J A 2006 Dual-field imaging polarimeter using liquid crystal variable retarders *Appl. Opt.* **45** 5470–8

[17] Azzam R M A 1982 Division-of-amplitude photopolarimeter (DOAP) for the simultaneous measurement of all four Stokes parameters of light *Opt. Acta* **29** 685–9

[18] Gori F 1999 Measuring Stokes parameters by means of a polarization grating *Opt. Lett.* **24** 584–6

[19] Kudenov M W, Escuti M J, Dereniak E L and Oka K 2011 White-light channeled imaging polarimeter using broadband polarization gratings *Appl. Opt.* **50** 2283–93

[20] Craven-Jones J, Kudenov M W, Stapelbroek M G and Dereniak E L 2011 Infrared hyperspectral imaging polarimeter using birefringent prisms *Appl. Opt.* **50** 1170–85

[21] Sabatke D S, Locke A M, Dereniak E L, Descour M R, Garcia J P, Hamilton T K and McMillan R W 2002 Snapshot imaging spectropolarimeter *Opt. Eng.* **41** 1048–54

[22] Zhao X, Bermak A, Boussaid F and Chigrinov V G 2010 Liquid-crystal micropolarimeter array for full Stokes polarization imaging in visible spectrum *Opt. Express* **18** 17776–87

[23] Arbabi A, Horie Y, Bagheri M and Faraon A 2015 Dielectric metasurfaces for complete control of phase and polarization with subwavelength spatial resolution and high transmission *Nat. Nanotechnol.* **10** 937–43

[24] Meinzer N, Barnes W L and Hooper I R 2014 Plasmonic meta-atoms and metasurfaces *Nat. Photonics* **8** 889–98

[25] Yu N and Capasso F 2014 Flat optics with designer metasurfaces *Nat. Mater.* **13** 139–50

[26] Yu N, Aieta F, Genevet P, Kats M A, Gaburro Z and Capasso F 2012 A broadband, background-free quarter-wave plate based on plasmonic metasurfaces *Nano Lett.* **12** 6328–33

[27] Pors A and Bozhevolnyi S I 2013 Plasmonic metasurfaces for efficient phase control in reflection *Opt. Express* **21** 27438–51

[28] Lin J, Mueller J P B, Wang Q, Yuan G, Antoniou N, Yuan X-C and Capasso F 2013 Polarization-controlled tunable directional coupling of surface plasmon polaritons *Science* **340** 331–4

[29] Lin D, Fan P, Hasman E and Brongersma M L 2014 Dielectric gradient metasurface optical elements *Science* **345** 298–302

[30] Kang M, Feng T, Wang H-T and Li J 2012 Wave front engineering from an array of thin aperture antennas *Opt. Express* **20** 15882–90

[31] Sun S *et al* 2012 High-efficiency broadband anomalous reflection by gradient meta-surfaces *Nano Lett.* **12** 6223–9

[32] Huang L, Chen X, Mühlenbernd H, Li G, Bai B, Tan Q, Jin G, Zentgraf T and Zhang S 2012 Dispersionless phase discontinuities for controlling light propagation *Nano Lett.* **12** 5750–5

[33] Chen W T *et al* 2014 High-efficiency broadband meta-hologram with polarization-controlled dual images *Nano Lett.* **14** 225–30

[34] Huang L, Chen X, Bai B, Tan Q, Jin G, Zentgraf T and Zhang S 2013 Helicity dependent directional surface plasmon polariton excitation using a metasurface with interfacial phase discontinuity *Light Sci. Appl.* **2** e70

[35] Fan R-H, Zhou Y, Ren X-P, Peng R-W, Jiang S-C, Xu D-H, Xiong X, Huang X-R and Wang M 2015 Freely tunable broadband polarization rotator for terahertz waves *Adv. Mater.* **27** 1201–6

[36] Benetou M I, Thomsen B C, Bayvel P, Dickson W and Zayats A V 2011 Four-level polarization discriminator based on a surface plasmon polaritonic crystal *Appl. Phys. Lett.* **98** 111109

[37] Drezet A, Genet C and Ebbesen T W 2008 Miniature plasmonic wave plates *Phys. Rev. Lett.* **101** 043902

[38] Afshinmanesh F, White J S, Cai W and Brongersma M L 2012 Measurement of the polarization state of light using an integrated plasmonic polarimeter *Nanophotonics* **1** 125

[39] Wen D *et al* 2015 Metasurface for characterization of the polarization state of light *Opt. Express* **23** 10272–81

[40] Pors A, Nielsen M G and Bozhevolnyi S I 2015 Plasmonic metagratings for simultaneous determination of Stokes parameters *Optica* **2** 716–23

[41] Xie Y-B, Liu Z-Y, Wang Q-J, Zhu Y-Y and Zhang X-J 2014 Miniature polarization analyzer based on surface plasmon polaritons *Appl. Phys. Lett.* **105** 101107
[42] Peltzer J J, Bachman K A, Rose J W, Flammer P D, Furtak T E, Collins R T and Hollingsworth R E 2012 Plasmonic micropolarizers for full Stokes vector imaging *Proc. SPIE* vol 83640 O-O-12
[43] Foreman M R and Török P 2010 Information and resolution in electromagnetic optical systems *Phys. Rev.* A **82** 043835
[44] Foreman M R, Macias-Romero C and Török P 2008 A priori information and optimisation in polarimetry *Opt. Express* **16** 15212–27
[45] Foreman M R, Favaro A and Aiello A 2015 Optimal frames for polarisation state reconstruction *Phys. Rev. Lett.* **115** 263901
[46] Pors A, Nielsen M G and Bozhevolnyi S I 2013 Broadband plasmonic half-wave plates in reflection *Opt. Lett.* **38** 513–5
[47] Zheng G, Mühlenbernd H, Kenney M, Li G, Zentgraf T and Zhang S 2015 Metasurface holograms reaching 80% efficiency *Nat. Nanotech.* **10** 308–12
[48] Ding F, Wang Z, He S, Shalaev V M and Kildishev A V 2015 Broadband high-efficiency half-wave plate: a supercell-based plasmonic metasurface approach *ACS Nano* **9** 4111–9
[49] Azzam R M A and Lopez A G 1989 Accurate calibration of the four-detector photopolarimeter with imperfect polarizing optical elements *J. Opt. Soc. Am.* A **6** 1513–21
[50] Vollmann T E A K 2015 *Spectroscopic Instrumentation—Fundamentals and Guidelines for Astronomers* (Berlin: Springer)
[51] Aiello A, Puentes G, Voigt D and Woerdman J P 2006 Maximum-likelihood estimation of mueller matrices *Opt. Lett.* **31** 817–9
[52] Lu S-Y and Chipman R A 1996 Interpretation of Mueller matrices based on polar decomposition *J. Opt. Soc. Am.* A **13** 1106–13